Geophysical surveys over and inside the Tobiotsuka Kofun – Okayama prefecture

(Article begins on next page)

07 January 2023

iris-AperTO

Geophysical surveys over and inside the Tobiotsuka Kofun – Okayama Prefecture.

Comina C.[1], Sotiropoulos P.[2], Maroulakis S.[2], Vacha D.[1], Mandrone G. [1], Masturzo N. [3], Matsumoto N. [4] and Seike A. [4]
[1]Dipartimento di Scienze della Terra, Università degli studi di Torino, Torino (IT)
[2]Terramarine, Athens (GR)
[3]Dipartimento di Studi Storici, Università degli studi di Torino, Torino (IT)
[4]Department of Archaeology, Okayama University (JP)

ABSTRACT
Burial mounds are artificially (or partially artificially) erected hills that cover a monumental tomb, usually in the form of a stone chamber. Different types of burial mounds are distributed worldwide and have built in different archaeologically interesting periods. Use of non destructive geophysical surveys for their study offer the opportunity to image their internal structure and evidence peculiar anomalies that can be later investigated with archaeological excavations, limiting invasiveness. The main innovative part of this work lies on the combined use of Ground Penetrating Radar and Electric Resitivity Tomography over and inside an unexplored burial site in Japan, the Tobiotsuka Kofun, a late Kofun period burial mound, dated approximately late 6th –early 7th century AD and located in the Okayama Prefecture. Effectiveness of the geophysical surveys is demonstrated by the correct imaging of known structures and by the combined evidence of the mound organization, which allowed to draw a reliable initial archaeological interpretation with evidence of several interesting excavation spots. The adopted methodologial surveying approach was verified as a valuable choice for investigations in similar archaeological settings.

Article Highlights:

- Effective use of Ground Penetrating Radar and Electric Resitivity Tomography is over and inside a late Kofun period burial mound;

- Geophysical evidences contributed to the better understanding of the structure of the Kofun and in the location of archeologically interesting zones where to focus the excavations;

- The adopted methodologial surveying approach verified as a valuable choice for investigations in similar archaeological settings.

Corresponding author: Cesare Comina, cesare.comina@unito.it

1. INTRODUCTION

The investigation of burial mounds structure, and the location of the tombs within the mound are very interesting archaeological tasks. The interest is relative both to the archaeological significance of the tomb itself, and its eventual content in term of artefacts, and to the fact that burial mounds are, by themselves, monuments of past human activity and offer opportunities to reconstruct important information about life and customs during the building period (see e.g. Bradley and Fraser, 2010; Renfrew and Bahn, 2000). Burial mounds commonly occur through the world, starting from the beginning of the Neolithic period (Hodder, 1984). They have been then erected in different periods of time, up to to Middle Ages, and, besides burial purposes, served also for habitation, ceremonial or even commemorative purposes (Barret, 1990; Tilley, 1994). The archeological research has followed specific directions in the classification of such structures based on their location, form and date of construction. Multiple terms have been introduced to express their worldwide distribution and their unique archeological, historical and architectural significance (Kipfer, 2000; Steinhaus and Knopf, 2018).

Ancient Japan is particularly characterized by distinctively large number of burial mounds, widely known as "Kofuns", this term also gives the name to a defined period of Japanese history: Kofun Period (3rd -7th century AD). The shape and size of these burial mounds show significant variation, that has been actively investigated by Japanese archaeologist to reconstruct social hierarchy and political relationships in ancient Japan (Tsude, 1987; Knopf et al., 2018). Keyhole-shaped mounds come at the top of the hierarchy. Construction of the bigger keyhole-shaped mounds culminated in the 5th century, and then declined in the Late Kofun period (6th - late 7th century AD). Preferential location of the mounds also changed from prominent positions to places more integral with the natural landscapes (Tembata, 2016). Among these later mounds there are a number of different shapes. The most common of the non-keyhole shapes are round and square mounds. Smaller rounded mounds are usually around 15-20 m in diameter. Also, from the late 4th century, the continental-style stone-chamber tomb with corridor entrance was introduced from Korea and becomes the most used tomb shape within the later Kofuns, especially during Late Kofun period. Most of these later burial mounds are still not investigated or surveyed so that archaeological significance of these constructions is still not completely understood.

The use of geophysical techniques for the non-invasive exploration of burial mounds can have therefore several potential applications, both in terms of geographical distribution and archaeological period investigated (in Japan and worldwide), and should be considered in order to guide archaeological excavations. This aspect is of paramount importance in the case of intact burial

mounds for which several cultures prescribe a limited possibility to explore the mound with invasive explorations. The investigation of burial mounds structure, and the location of the tombs within the mound is nevertheless a challenging geophysical task. Effectiveness of the geophysical surveys strongly depends from the relevant topography of the mound, state of vegetation, the used building material and the contrast between this and the eventual stone chamber. The superimposed mound filling material usually consist of soil, sand and gravel, eventually local boulders, comprising a complex stratigraphy. These heterogeneous materials are laid in layers of irregular thicknesses and geometries and can cause substantial heterogeneities in the resulting geophysical map. Among the different geophysical methods the more used for the exploration of burial mounds are Ground Penetrating Radar (GPR) and Electric Resistivity Tomography (ERT). Several successful applications of these methodologies can be found in literature (e.g. Zhao et al., 2015; Papadopoulos et al., 2010; Tonkov et al., 2006; Pipan et al., 2001). The GPR method was first employed for archaeological investigations in Japan, in 1982, and since then it was further applied at various archaeological sites (Nishimura and Goodman, 1998). Particularly, Nishimura et al. (1993) applied the GPR time slice method to Nagatsuka Kofun, in Ogaki-shi, revealing the existence and general shape of a moat. A ground radar survey was also applied at the Kanmachi Mandara burial ground, in Nakakima Machi, Ishikawa Ken, where a keyhole-shaped burial mound of the early Kofun period was found (Goodman and Nishimura, 1993). Some of the earliest and bigger Japanese Kofuns have been already investigated with geophysical techniques (Goodman et al., 2009 and 2006) and some application of these methodologies to Japanese Kofuns and tombs are present in literature (e.g. Edwards et al., 2000; Kamei et al., 2000). Particularly Edwards et al. (2000) applied radar and resistivity surveys at the Saitobaru Tomb Cluster Site, in Miyazaki, in order to locate the tomb for which no visible surface markers were available. Several authors also discussed on the best surveys disposition in order to obtain increased resolution in the imaging of the internal structure of a burial mound and of the inside stone chamber (Chen et al., 2018; Tsourlos et al. 2014) and alternative surveys combinations and methods (e.g. Forte and Pipan, 2008) .

In this paper geophysical surveys executed over and inside a late Kofun period burial mound, the Tobiotsuka Kofun, are reported. Both GPR and ERT surveys have been executed in the framework of a research project (BE-ARCHAEO, "BEyond ARCHAEOlogy: an advanced approach linking East to West through science, field archaeology, interactive museum experiences" EU project) which foresees devoted excavations and archaeological activities on the basis also of the geophysical evidence.

The major aims of the geophysical investigations were therefore:

(i) to reconstruct the structure of the burial mound and eventually the construction stages;

(ii) to evaluate the effectiveness of ERT surveys in identifying the stone chamber and investigate stone chamber walls by means of GPR;

(iii) to investigate the stone chamber floor in order to suggest possible preferential archaeological excavations locations.

In the end, GPR 2D radargrams and time slices, ERT 2D sections and 3D GPR and ERT images, contributed to the better understanding of the structure of Tobiotsuka Kofun and in the location of archeologically interesting zones of the mound where to focus the excavations.

2. TOBIOTSUKA BURIAL MOUND

The Tobiotsuka Kofun is a late Kofun period burial mound, dated approximately late 6th –early 7th century AD, located in Okayama Prefecture (**Figure 1**). In the southern part of Okayama huge burial mounds, including the Zozan kofun, the 4th largest mound in Japan with 350m in the major axis (Niiro, 2012), were constructed from the 5th to the 6th century, showing that powerful families dominated the area. Previous studies indicated that the local chiefs were sometimes in close ties with the central polity in the Kinai area, and sometimes come into collision with it. It is highly probable that the Tobiotsuka Kofun is the last of the succession of chiefly burial mounds in the area. Investigations of the Tobiotsuka Kofun is therefore expected to clarify the activities of the powerful family at the final phase of the Kofun period and shed new light on how culture, society and political relationships changed in this critical period of ancient Japanese history.

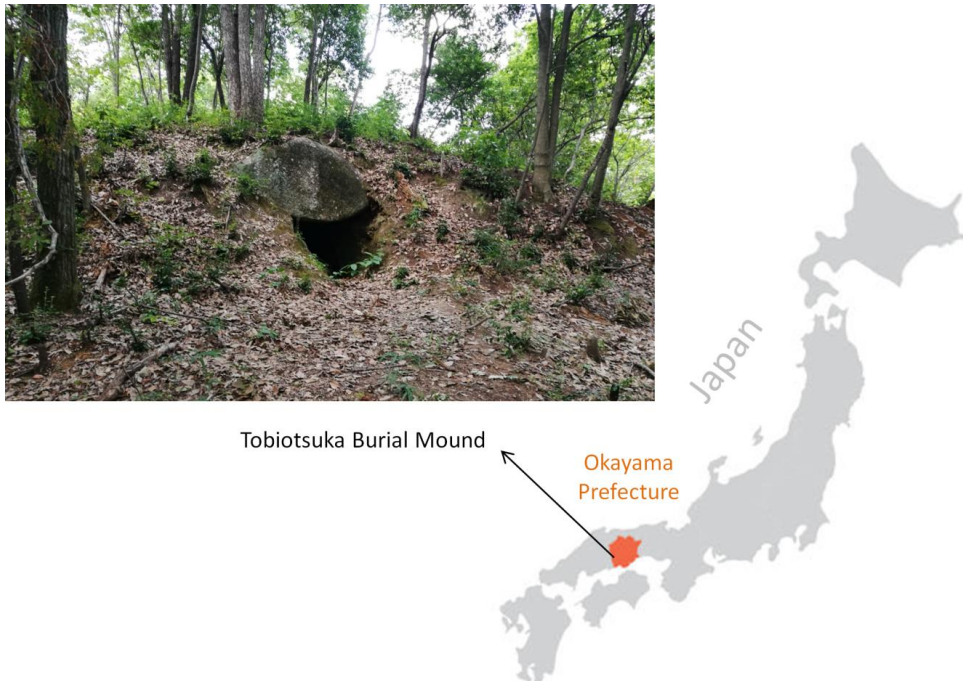Tobiotsuka Burial Mound

Okayama Prefecture

Japan

Figure 1 – Location of the Tobiotsuka Burial Mound within Japan, in the Okayama prefecture and picture of the entrance of the stone chamber with evidence of the relevant vegetation over the mound.

The area surrounding the Tobiotsuka Kofun geologically pertains to the Kibi plateau sector, composed of eroded hilly land surfaces, interrupted by steep younger incisions, and with an elevation between 200 m and 600 m a.s.l. This sector connects the Chugoku Mountains (1729 m a.s.l. max height), located to the north, and the Seto Inland seaside plane, to the south (Suzuky, 1996). The study area is located at the foot of a small hill.

Previous topographic surveys (Seike et al., 2019) over the Tobiotsuka Kofun evidenced an approximately rounded shape for the mound with an average diameter of about 23 m, and a maximum

height from the floor of the stone chamber of about 3 m. The resulting topographic map (**Figure 2**) has been obtained by measuring the two reference points (GPS1 and GPS2) with GNSS, with an error range of less than 2.0 cm in both horizontal and vertical directions. Other reference points were then measured by closed traverse surveys with a fractional closing error of 1/3700. Total stations were used to draw topographic map with 25 cm contour intervals, more than 800 measurements where performed to obtain the final topographic map.
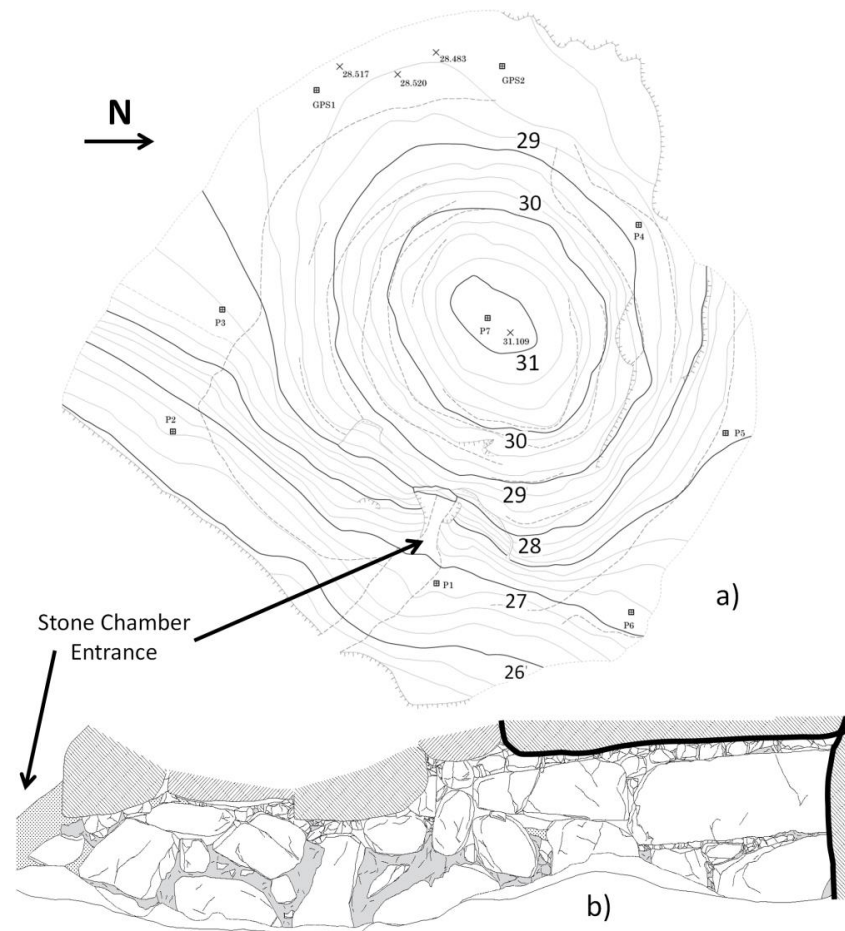

Figure 2 – Previous topographic investigations (Seike et.al.,2019) over the Tobiotsuka Burial Mound: a) topographic map of the mound with evidence of topographic reference points (P1 to P7 and GPS1,2) b) east side wall of the stone chamber with evidenced with thick black contouring the most significant stone blocks located towards the end of the stone chamber at the ceiling and in the back wall.

The burial mound is covered by dense vegetation (**Figure 1**) including trees and shallow bushes. The stone chamber within the mound is open and accessible by means of a shallow (about 1 m heigth) hole in the east side of the mound, with a stone block placed on top of the entrance (**Figure 1**). The stone chamber (**Figure 2b**) is composed of big stone boulders and is approximately 12.5 m long with a variable height from the entrance to its end (where it is about 2 m high). The most significant stone

blocks are located towards the end of the stone chamber at the ceiling and in the back wall (see the thick black contouring of the main blocks in **Figure 2b**).

Geologically the basement of the study area is composed of the Permian Maizuru group (Suzuki 1996), mainly represented by mudstone undergone to contact metamorphism, sandstone and basalts. In those formations Cretaceous and Paleogene volcanic rocks are intruded. In particular in the area the major outcrops are composed by (**Figure 3**): medium to coarse- grained granodiorite and tonalite (Dq), hornblende-biotite (Ghb), granodiorite and granite, biotite granite (Gb). Unconsolidated, loose alluvial deposits (a), composed mainly of gravel and sand, are located in the channel and flood plains of the Takahashi and Mae Rivers.
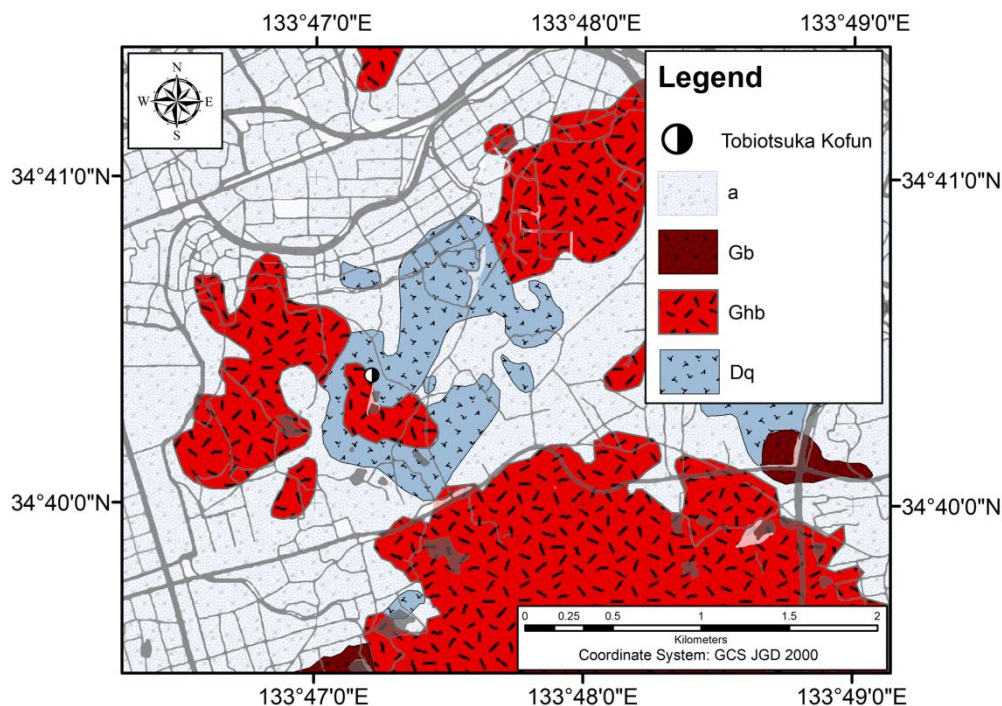

Figure 3 – Geological sketch of the study area. Legend: a: recent alluvial deposit; Gb: Biotite Granite; Ghb: Horneblende Biotite Granite; Dq: Granodiorite and Tonalite. (redrawn from Akagi, 1927 and Matsuura et al. 2002).

Given the above described general geological setting, the local geological/soil conditions around the area of mound are the ones that would more influence the geophysical tests. According to the World Reference Base (WRB) soil correlation system (Deckers et al., 2001), the soil profile in the study area is constituted by mainly Leptic and/or Haplic Cambisol soils. These type of soils are at the beginning of soil formation, with a weak horizon differentiation and weak, mostly brownish, discoloration and/or structure formation in the soil profile. The grain size of the shallow soil is mainly sandy to loamy and has a greyish brown color with good drainage.

3. DATA ACQUISITION

Geophysical surveys were executed in the period from February 28th to March 7th, 2019. Both GPR and ERT surveys were designed and implemented to meet the scope of work in terms of mapping with the potential best analysis and depth coverage the area under study. The surveys were designed taking into account the access limitations due to dense forestation and steep topography of the site (see **Figure 1 and 2**). Location of the different survey lines was performed on site with respect to available topographic reference points permanently installed on site after previous topographic measurements (see **Figure 2**). For GPR and ERT analyses the topographic map of the mound was digitized and interpolated at 0.5 m spacing (**Figure 4**). Contemporary to geophysical data acquisition also a photogrammetric analysis of the inside of the stone chamber was performed. This resulted in a photogrammetric georeferenced point cloud that was used to constrain the geophysical results and to discuss the geophysical evidence.
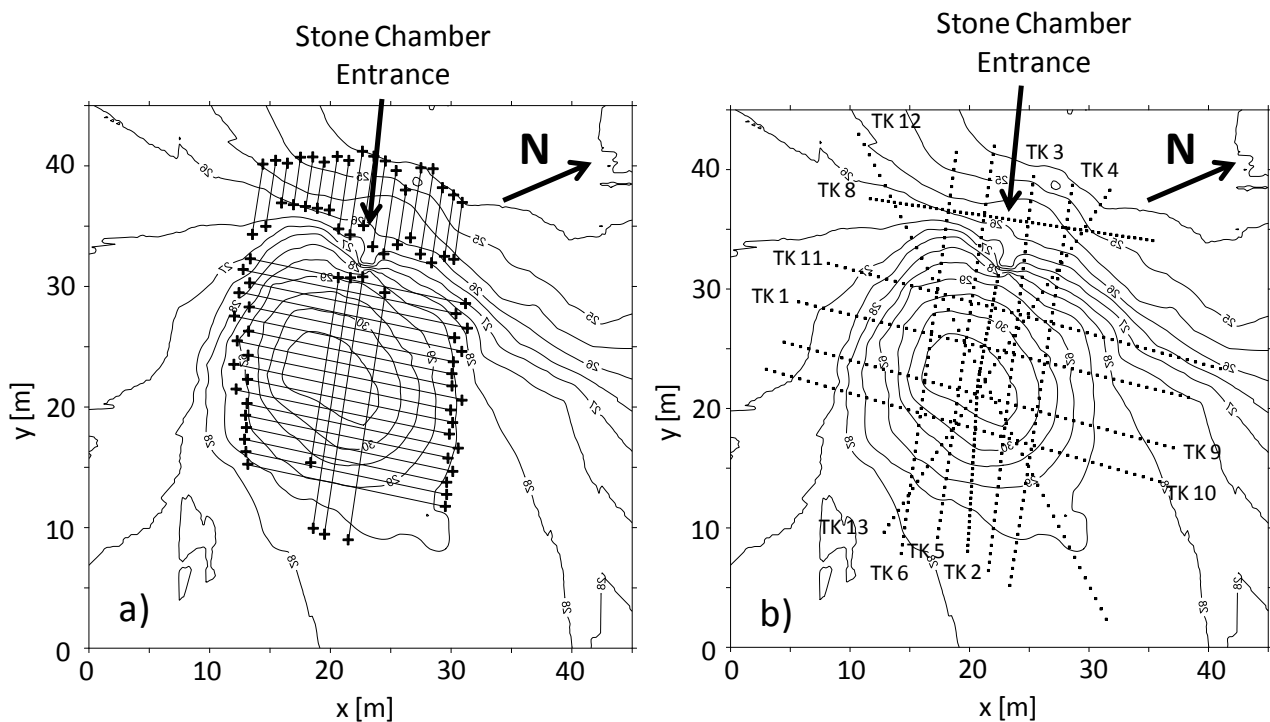
Figure 4 – Geophysical survey lines over the Tobiotsuka burial mound: a) GPR surveys and b) ERT surveys; evidence of the steep site topography and of the reference topographic points is also reported.

The photogrammetry of the interior of the burial chamber was based on 21 control points. This high number of control points was necessary due to difficulties in overlapping the series of 250 photos in the narrow space of the chamber, despite the use of 20 mm lens on a full frame camera (former 35 mm format). One of the main problems was the use of a balanced lighting, solved using a line of

lamps first on one side of the chamber and after on the other one, to make an uniform level of lighting on the opposite stone surfaces. The resulting photogrammetric model had satisfying median projection error of 4.8 [px].

2.1 GPR data acquisition

The GPR data were collected by means of a survey grid composed of 40 profiles with varying length (for a total length of 500 m), on the outer part of the mound, with an approximate distance among the profiles of 1 m (**Figure 4a**). Indeed due to the dense vegetation over the mound it was not always possible to strictly follow the predefined grid, therefore we judge on an approximate distance among profiles. A total of 38 profiles with varying length (for a total length of 161 m) were also acquired inside the stone chamber. Particularly the floor, walls, back wall and ceiling of the stone chamber have been tested with grids of parallel radargrams, almost every 0.35 m. Data were acquired with a Malå Groundexplorer system with a 450 MHz antenna. For all the profiles an odometer was adopted for determining the profile increment. Acquisition parameters were: sampling frequency of 5120 Hz, trace spacing of 0.01 m and time window of 86.3 ns.

2.2 ERT data acquisition

The ERT data have been acquired over the mound along 12 different survey alignments (TK1 to 6 and TK 8 to 13 in **Figure 4b**): 5 parallel to the main axis of the stone chamber; 4 cutting the main axis of the stone chamber; 2 crossing the main axis of the stone chamber; 1 in front of the entrance of the stone chamber. One additional profile (TK7) was also acquired inside the stone chamber in the middle of its floor.

For the surveys, an Iris Syscal R1 acquisition device was adopted with 48 measuring electrodes. Different electrodes spacings were used, depending on the available space and topographic constraints (ranging from 0.5 to 1 m). Different acquisition sequence approaches were also used, eventually combined in a single dataset to improve lateral resolution and investigation depth. The first adopted acquisition sequence was based on a Wenner-Schlumberger (WS) quadripole configuration and involved a total of 935 potential measurements along the section. This was aimed at increasing the penetration depth and detail of the surveys. For some of the survey lines the same WS acquisition sequence approach was used but with a reduced number of measuring quadrupoles (WSS - 544 potential measurements). This was aimed at reducing the acquisition time for some of the survey lines. The second adopted acquisition sequence was based on a Dipole-Dipole (DD)

quadripole configuration and involved a total of 542 potential measurements along the section. This was aimed at increasing the lateral resolution of the surveys.

4. DATA PROCESSING

Data acquired with the different geophysical instrumentations were largely processed independently by TERRAMARINE for GPR data and by DST-UNITO for ERT data. This independent processing approach was used to avoid biasing and cross-influences among the interpretations. Only after a satisfying processing was reached the combined results of GPR and ERT were discussed and uniformed in order to obtain a consistent imaging for all the surveys.

3.1 GPR data processing

Raw GPR data were analysed and processed with GPR-Slice software (Goodman et al, 1995; Goodman et al., 2004). The processing steps included relatively standard methodological approaches: data/trace editing and 'rubber-band' interpolation; topographic correction; dewow filtering; time-zero correction; band pass filtering; background removal; velocity analysis and depth conversion, with an automatic hyperbola fitting procedure (typical hyperbola fitting resulted in a GPR velocity of 9.9 cm/ns); AGC (Automatic Gain Correction), with an automatic gain function applied to each trace based on the difference between the mean amplitude of the signal in a particular time window and the maximum amplitude of the trace as a whole.

Processed radargrams were finally Hilbert-transformed, in order to eliminate phase components before assembling the dataset and compiling 3D vector volumes.

3.2 ERT data processing

Experimental ERT data were processed and inverted with two different inversion approaches: along the 2D lines with Res2DInv (Geotomo Software), and in a global 3D inversion with ERTLab (developed by Multi-Phase Technologies and Geostudi Astier). For both approaches, topographic data from already available topographic measurements were essential for obtaining terrain elevation at each electrodes positions (see **Figure 4b**) with Surfer (Golden Software) and ArcGIS suite (Esri). Before both inversions the filtering of measured apparent resistivity data, after incorporation of topographic information, consisted of removing: measurements with an instrumental standard deviation greater than 5%; quadrupoles belonging to badly ground-coupled electrodes; quadrupoles with transmitted currents lower than 0.1 mA; quadrupoles with potential's difference at the receivers lower than 0.1 mV; negative apparent resistivity values; apparent resistivity values higher than 100,000 Ohm.m.

For 2D inversions a "Robust Constrain" approach has been adopted in order to allow the algorithm to search for localized anomalies related to the presence of the stone chamber and other eventual anthropic evidences along the lines. A very good convergence of the results was obtained from the inverted resistivity models with a global r.m.s. (root mean square error) always below 2%. Inverted resistivity data were then elaborated with Surfer (Golden Software) in order to image resistivity variations along the survey lines with a uniform color scale and with Voxler (Golden Software) in order to visualize in 3D the 2D resistivity results and compare with 3D resistivity inversions.

For 3D inversions, after the above-mentioned filtering, a total of 15318 potential measurements were available. The inversion approach of these data was then based on a linearization procedure requiring a "starting" model, and on regularization based on the Tikhonov's strategy (Tikhonov and Arsenin, 1977), where the condition of minimum roughness of the model is used as stabilizing function (Constable et al., 1987). Throughout the inversion iterations, the effect of non-gaussian noise is also appropriately managed using a robust data weighting algorithm (LaBrecque et al., 1996; Morelli and LaBrecque, 1996). A starting model with a background resistivity, obtained as the mean of measured apparent resistivities (450 Ohm.m) and an incorporated high resistivity anomaly (50.000 Ohm.m) in the known location of the stone chamber was adopted. A 0.5 m mesh discretization was used; this choice was based on the sensitivity of the chosen electrodes disposition (see later in the discussion section). Few iterations were necessary to achieve the convergence of the inversion process from the constructed starting model. The misfit between calculated and measured potentials was on average within a 5 % discrepancy, apart from a few outliers. Inverted resistivity data were then visualized with ERTLabViewer and further elaborated with Voxler (Golden Software) in order to visualize the 3D resistivity distribution and to compare it with 2D inversions.

Given the different inversion approaches adopted (robust constrain for 2D inversion and smoothness constrain for 3D inversion) the results from the inverted models will be only partially comparable. The different inversion approaches were specifically adopted to take advantage of the potentialities of the two methods in the data interpretation. In particular, 2D robust constrained inversion will allow a more sharp definition of the anomalies along the survey lines. However this can be considered reliable only when the current flow is mainly 2D, i.e. when the anomalies are elongated in perpendicular direction with respect to the survey line. The 3D smoothness constrained inversion will conversely allow to extend spatially the information measured along the lines, taking into account of a more reliable 3D current flux particularly when the anomalies are aside the survey lines.

5. RESULTS

The GPR and ERT data processing and analysis was followed by a visualization and interpretation stage as well as the correlation of potential targets derived from both methods. The main concept is to overcome the restriction of each method and work complementary to provide "valuable info" to archaeologies and geoscientists collaborationg in the framework of the project. Hereafter the main results of the two surveys are presented independently, they will be later combined and discussed together in the discussion section.

4.1 GPR results

Results obtained along radargrams acquired in the stone chamber floor evidenced multiple reflections and diffraction hyperbolae towards the entrance of the stone chamber. These features are evidenced in **Figure 5** along one of the radargrams by a red square. These anomalies can be potentially correlated with the presence of stone boulders or more compacted material at the entrance.
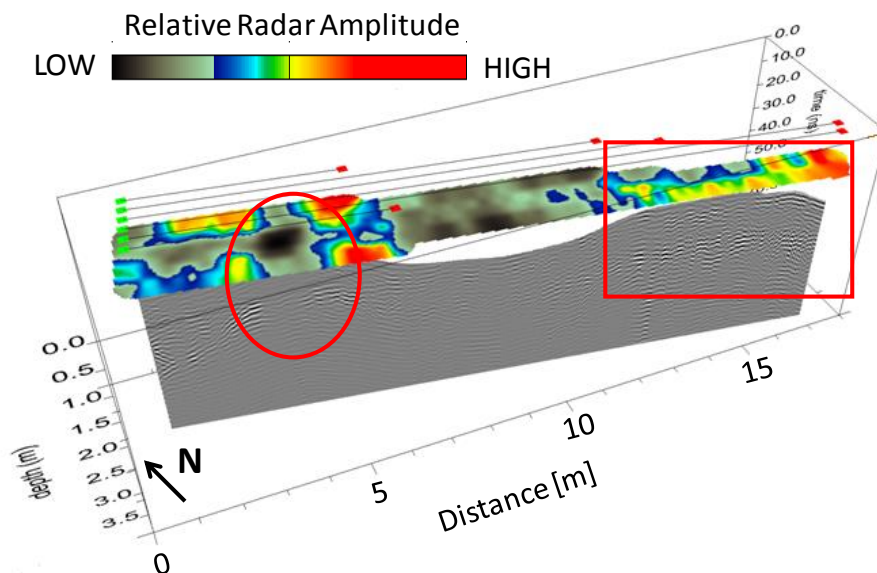

Figure 5 – 3D image of the GPR amplitude map for the relative depth of 0.7 m below the floor of the stone chamber together with an example radargram, with topographic correction. Reflection features described in the text are identified in red.

Another interesting anomaly has been identified, along the ne chamber floor, right down and near to the back wall of the chamber. This potential target is depicted **Figure 5** along one of the radargrams by a red oval. This anomaly evidence as a zone in the radargrams where the continuity of the reflection path is interrupted and the evidence of clear localized reflection anomalies is observed. The zone related to the presence of this target can be indicated at about 0.7 m depth for a length of about 2 m.

This target can be correlated with the presence of a solid rock body or with the presence of some alteration in the continuity of the reflections due to soil reworking.

On the top of **Figure 5** an amplitude depth slice (at 0.7 m from the surface) the combination of all the lines acquired on the floor of the stone chamber is also reported. From this image, it can be observed that the first of the above-described anomalies appears as a high amplitude area while the second one as a low radar amplitude zone surrounded by higher amplitude zones.

From the radargrams acquired along the walls of the stone chamber (**Figure 6**) it is possible to evidence the presence of strong reflection events at depths behind the walls ranging from 0.8 to 1.2 m. These events are continuous along the walls (dashed red line in **Figure 6**) and can be associated with the end of the stone blocks used to build the stone chamber and therefore to their thickness. It can be observed also that the continuity of these events is not always preserved due to the presence of diffraction hyperbolae which are observable at the transition from one block to the other. More continuous and clear reflections are obtained for the bigger stone blocks towards the end of the stone chamber (see **Figure 6**). Same reflections are observed in the radargrams acquired along the ceiling of the stone chamber, evidencing a similar width of the blocks.
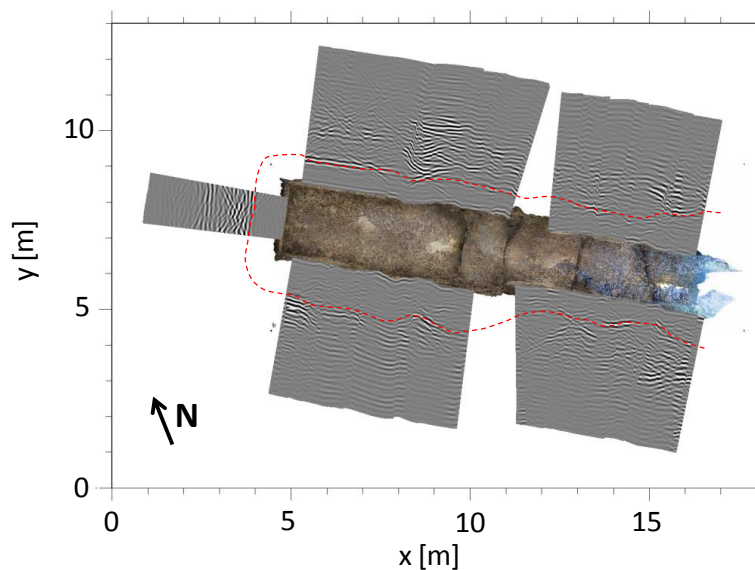

Figure 6 – Vector projection of different radargrams taken on the vertical walls of the stone chamber, evidence of the main reflections due to the end of the stone blocks constituting the stone chamber is also reported with a dashed red line. The photogrammetric point cloud of the stone chamber is also reported.

As it can be evidenced in **Figure 1** rough terrain due to dense forestation and relevant topography caused many difficulties during GPR data acquisition on the outer part of the mound partially compromising data quality. Nevertheless satisfactory imaging of interesting high amplitude reflection zones was possible through GPR amplitude maps compiled from all the acquired data. **Figure 7**

report, as an example, a 3D image of the GPR amplitude map with evidence of the GPR grid lines on the outer part of the mound. From this Figure, it is possible to evidence the continuity of the high amplitude reflection events depicted from the profiles acquired at the floor of the stone chamber towards its exit (red square in **Figure 5**).

Figures 8 report 3D amplitude maps for two different depth slices below the surface of the mound. From the shallower depth slice (0.5 – 1 m depth in **Figure 8a**) it is possible to evidence the presence of a high amplitude anomaly, approximately below the top center of the mound (white dashed circle). This anomaly is apparently too shallow to be directly correlated to the stone chamber and could therefore suggest the presence of a circular feature at the central top part of the mound (stone boulders or bigger stone blocks on the top of the ceiling of the stone chamber). From the deeper depth slice (2.1 – 2.5 m depth in **Figure 8b**) it is possible to evidence the presence of a linear feature (white rectangle) matching in terms of depths and dimensions to the rock construction of the stone chamber. Beside the known feature of the stone chamber, the evidence of high amplitude reflection zones is also depicted near the entrance of the stone chamber (dashed white line).
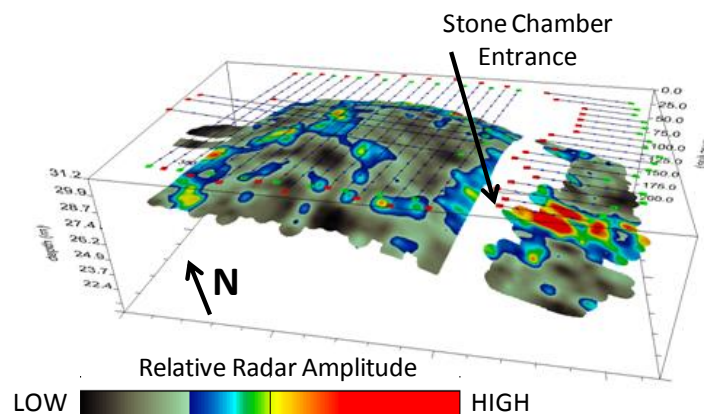

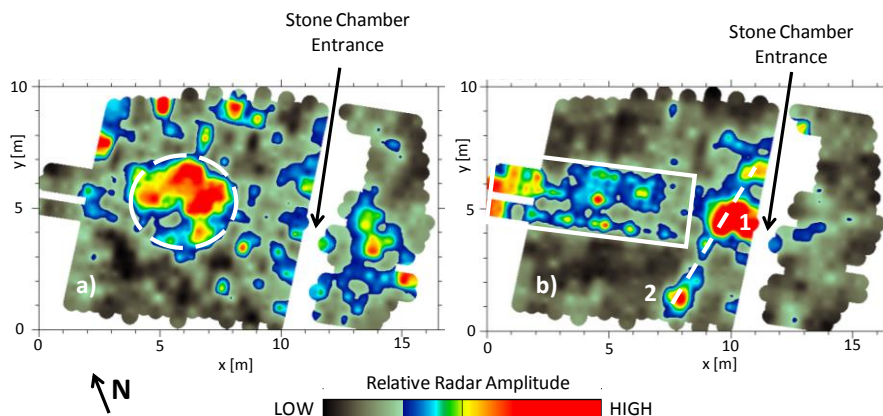**Figure 7: 3D image of the GPR amplitude map with evidence of the GPR grid lines.**

Figure 8: 3D image of the GPR amplitude map for the depth ranges of a) 0.5-1 m and b) 2.1-2.5 m; evidence of the anomalies described in the text is also provided.

These last high amplitude zones appear to be aligned along a defined direction. The bigger anomaly (1 in **Figure 8b**) could be related to the presence of the big stone blocks at the entrance. The smaller anomaly (2 in **Figure 8b**) in the bottom of the figure does not have instead any particular evidence on site and could be an interesting excavation spot.

4.2 ERT results

The most relevant results from 2D ERT inversions were obtained along the survey lines cutting the stone chamber axis (**Figure 9**). Along these lines, it is possible to recognize several features related to the structure of the mound and to the stone chamber. Particularly, the presence of the stone chamber is depicted with high resistivity values related to the air void inside the chamber (resistivity higher than 2000 Ohm.m) and to the surrounding rocks (resistivity between 1200 and 2000 Ohm.m). The stone chamber dimensions and location following these resistivity ranges are highly comparable with the real dimensions and shape of the chamber.
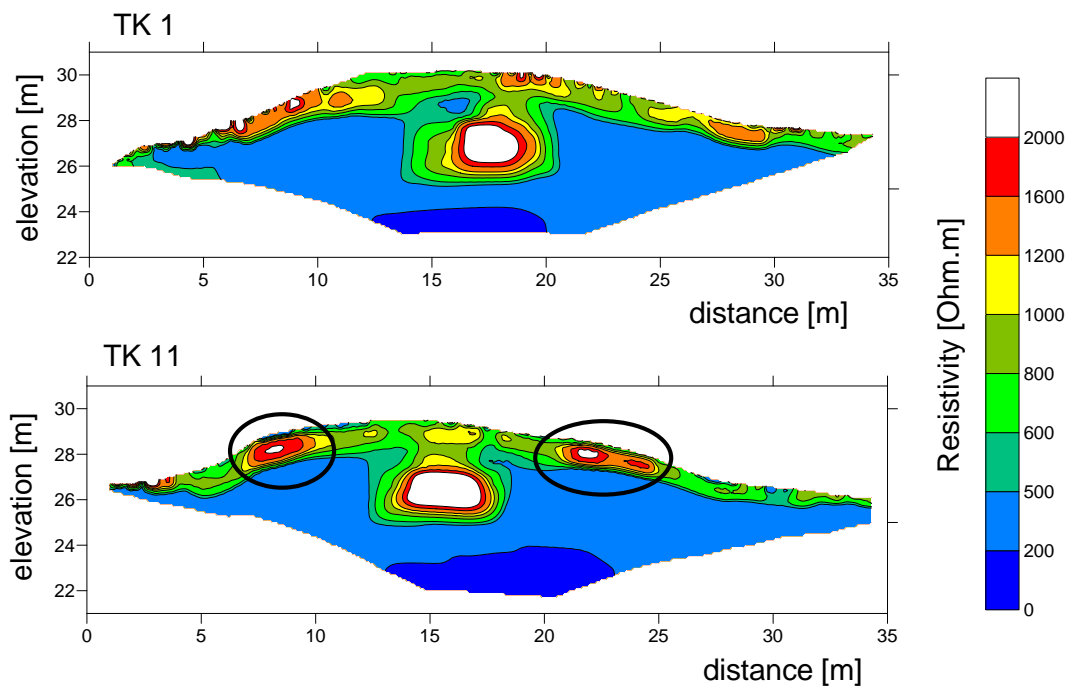

Figure 9: Inversion results of two of the 2D resistivity lines cutting the stone chamber axis with evidence of two relevant high resistivity anomalies (black circles).

Along the same lines it can be also noted the reduced stone chamber height along line TK 11, which is located more towards the entrance, with respect to TK 1 (see **Figure 4b**). The stone chamber appears surrounded, with a sharp lateral and vertical transition, by a material with uniform and relatively low resistivity (around 200 Ohm.m) judged to be related to the natural hill. Above the stone chamber and the natural hill a shallow coverage with higher resistivity (between 600 and 800 Ohm.m) about 1 m thick is observed along all the survey lines. Within this shallow coverage localized high resistivity anomalies (resistivity between 1000 and 2000 Ohm.m) are evidenced, these can be related

to the presence of the roots of the threes or to localized stone boulders placed on site to cover the natural hill in some specific positions of the mound.

Of particular interest are the two, almost symmetric, high resistivity anomalies, observable along the line TK 11 (black circles in **Figure 9**). These anomalies appear to be located in the changing slope position of the mound and therefore could suggest the presence of stone boulders put in place along the top ring of the mound to preserve the mound shape. The rightmost of these anomalies appear less compacted with respect to the left one. This evidence is also related with a reduced slope descent on the left part of the mound and could suggest partial sliding of this side of the mound, which could have consequentially relaborated the stones in this location.

Another interesting result was obtained with the survey line (TK 7) conducted inside the stone chamber (**Figure 10**). The resistivity distribution along this line confirm the presence of the natural hill at depth (resistivity around 200 Ohm.m).
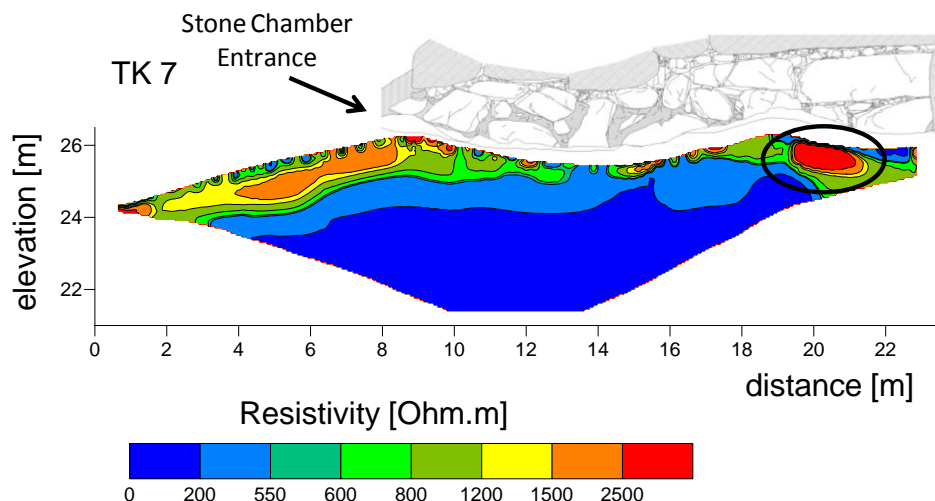

Figure 10: Inversion results of the 2D resistivity line executed inside the stone chamber (TK7) with evidence of the high resistivity anomaly towards the chamber end (black circle) and the stone chamber wall.

Towards the entrance of the stone chamber a shallow high resistivity coverage (resistivity between 1500 and 2500 Ohm.m) is also reported. This coverage can be related to the presence of more compacted material at the entrance of the stone chamber. This result is comparable with the high amplitude GPR anomalies already depicted in the same location (**Figure 7**). Towards the end of the stone chamber, a localized high resistivity anomaly (resistivity higher than 2500 Ohm.m) is also observed (the black circle in **Figure 10**). This last anomaly has a length of about 2 m and a thickness of about 1 m and appears to be covered by a reduced thickness (about 0.5 m) of lower resistivity material. Again this anomaly compares well with an analogous anomaly depicted by GPR in the same location.

From the inverted 3D resistivity distribution similar considerations already made on the 2D survey lines over the mound can be made. In particular, nevertheless the smoothness constrain adopted, a similar resistivity distribution within the mound is evidenced, comparable to what already commented in relation to the 2D results. Example results are reported in **Figure 11**.
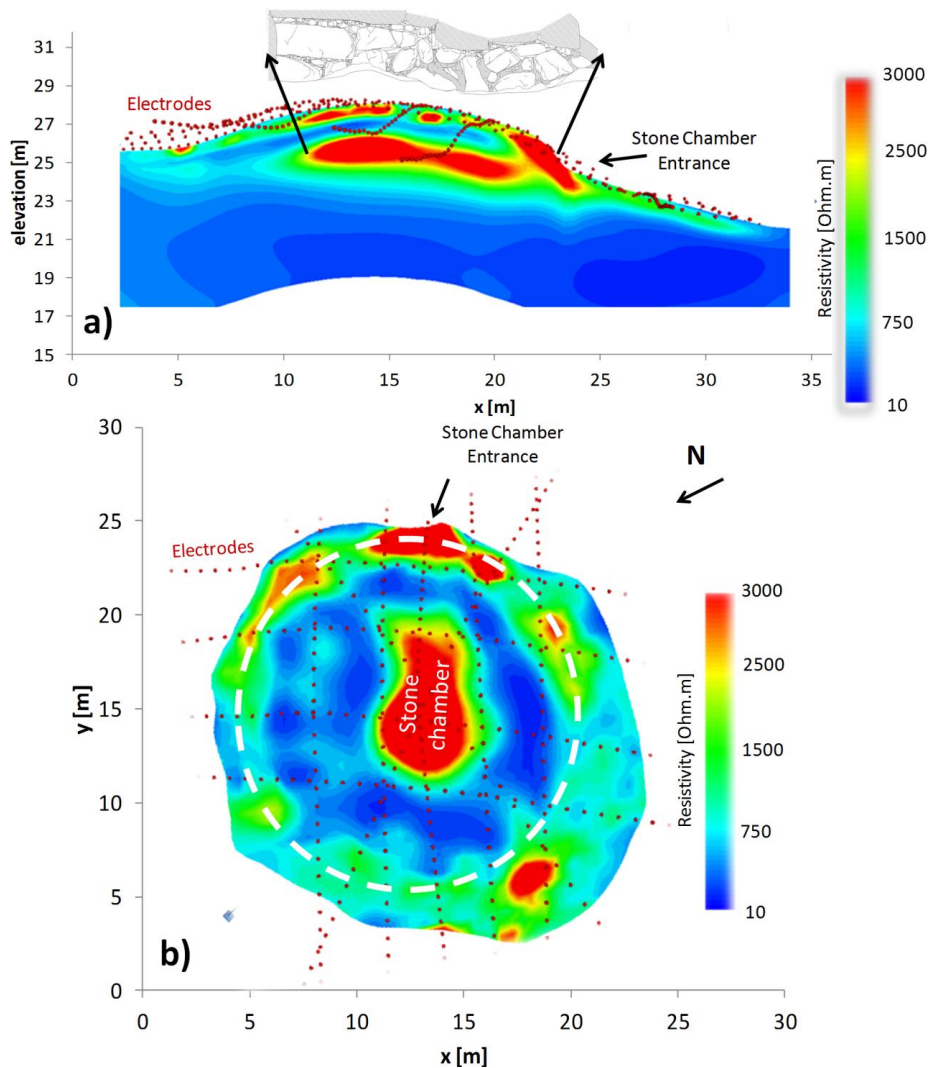

Figure 11: 3D visualization of the 3D inversion results: a) section of the 3D model in correspondence of the middle of the stone chamber with correspondence of the stone chamber location and dimensions and b) section of the 3D model at 28.5 m of elevation with evidence of the stone chamber location and localized high resistivity anomalies distributed along a crown ring (dashed white line).

High quality of the 3D inverted resistivity model is demonstrated by the very good correspondence of the high resistivity anomaly (resistivity above 2000 Ohm.m) inside the model with the known location of the stone chamber. With this respect **Figure 11a** reports a section of the 3D model in correspondence of the middle of the stone chamber. The shape of the high resistivity anomaly here

represented well reflect the shape of the stone chamber, with a reduced chamber height toward the entrance. Also, the presence of stone blocks placed at the entrance is clearly depicted by the data. With respect to the localized anomalies observed in the changing slope position in **Figure 9**, 3D inversion results help in establishing a lateral continuity of these anomalies. Particularly **Figure 11b** report a resistivity section of the 3D model at the elevation of 28.5 m. From this section is it possible to visualize the distribution of local high resistivity anomalies (resistivity higher than 2500 Ohm.m) along a more or less continuous ring (dashed white line) around the stone chamber location. The presence of these anomalies, and particularly of the one at the left of the entrance of the stone chamber, compare well to similar GPR anomalies.

6. DISCUSSION

Significant deductions and hypothesis can be performed on the geophysical surveys evidences. Particularly, GPR surveys along the walls of the stone chamber where highly effective in delineating the stone blocks dimensions and providing insights on the stones alignments and construction characteristics (**Figure 6**). GPR surveys were valuable nevertheless the relevant walls irregularities and the difficulties in establishing a proper surveying grid. The width of the blocks of the stone chamber is also acceptably well depicted by ERT surveys, given their lower resolution properties (see also **Figure 9**). In **Figure 12a and b** a comparison is made between the continuous radar reflection line (dashed red line) and the borders of an isosurface representation, at 550 Ohm.m, of the ERT results.
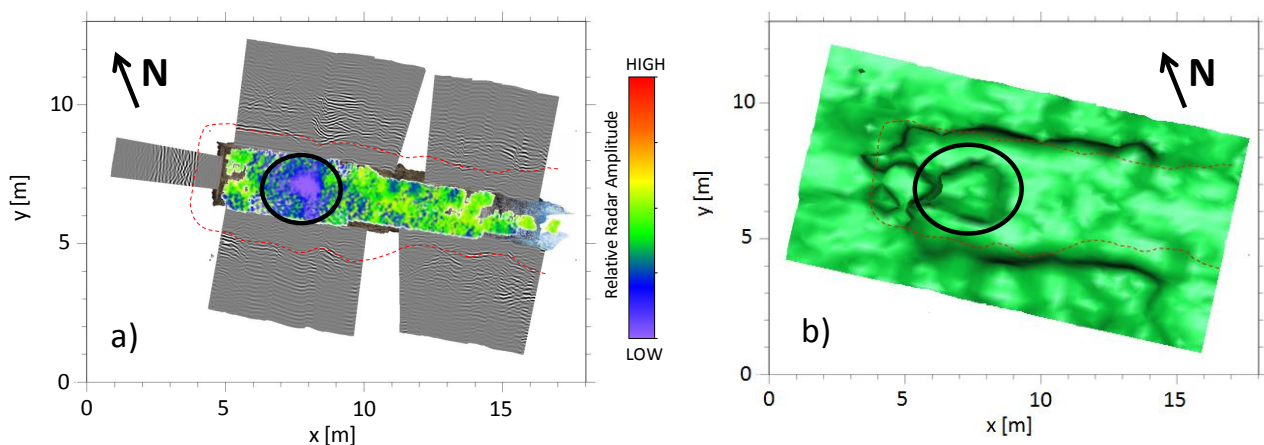

Figure 12: Main geophysical surveys results inside the stone chamber: a) GPR surveys with evidence of the continuous reflections due to the end of the stone blocks (dashed red line) and GPR amplitude map, cut to low amplitudes threshold, on the floor of the stone chamber; b) ERT surveys with 550 Ohm.m isosurface representation and superimposed continuous

reflection from GPS survey (dashed red line). In a) and b) the anomaly discussed in the text is evidenced with a black circle.

It can be noted that the two surveys compare promisingly well in the identifications of the stone blocks borders and in defining the width of the stone chamber. This was possible in the specific site given the high contrast between the blocks of the stone chamber and the surrounding material of the mound. Given this sharp contrast it can be deduced that the stone blocks were putted in place within the base of the natural hill with a reduced excavation effort and that no other stones or boulders were places behind the bigger blocks of the stone chamber.

Inside the stone chamber both GPR and ERT surveys evidenced also high amplitude diffraction anomalies (**Figures 5**) and high resistivity shallow coverage (**Figure 10**) towards the entrance of the tomb. The presence of these anomalies may suggest a sort of stone path or pavement built in order to get access to the Kofun. The continuity of this high amplitude and high resistivity zones also outside the stone chamber (**Figures 7 and 10**) corroborates this hypothesis.

More interestingly both surveys evidence the presence of a low reflection amplitude (**Figures 5**) and high resistivity anomaly (**Figures 10**) in the centre of the stone chamber towards its end. This anomaly is better represented in **Figure 12** (black circle) reporting the GPR amplitude map, cut to low amplitudes threshold (**Figure 12a**), and the ERT isosurface representation (**Figure 12b**). The combined interpretation of this anomaly may suggest the presence a stone block (eventually coffin) putted in place after a shallow soil reworking. Hypothesis for the nature of this anomaly are intriguing but can be only speculative and need verification by means of excavations.

Over the mound the results from 3D ERT survey clearly delineated the presence, spatial dimensions and location of the known stone chamber. For the present survey this task was not an issue since the stone chamber itself was accessible and dedicated photogrammetric analyses were performed in its inside. However, the effectiveness of the ERT survey, given also the complicated logistic conditions on the surface of the Kofun, are comforting with respect to the applicability of the ERT technique in similar environments. Specifically, as already reported in literature papers dealing with similar applications (e.g. Papadopoulos et al., 2010 and Tsourlos et al., 2014), ERT surveys adopted over other still not open and/or not discovered burial mounds could be effective in detecting the presence of the burial chamber, and its structure, with a completely non destructive approach. These surveys would therefore offer an image of the structure of the burial mound for eventual later exploration. Specifically the vertical and lateral heterogeneities due to the different layers inside the mound and the stone chamber anomaly were identified by the combined application of WS and DD acquisition sequences with improved accuracy. The use of the two different acquisition sequences along the same

survey line allowed an increase of both vertical and lateral resolution with limited acquisition effort. This result is in line with literature evidence on the performance of the different acquisition arrays (e.g. Papadopoulos et al., 2010).

The use of the two different inversion approaches (robust constrain for 2D inversion and smoothness constrain for 3D inversion) resulted effective in taking advantage of the potentialities of the two methods. Specifically 2D robust inversions allowed a detailed definition of the stone chamber structure along the profiles cutting perpendicularly the stone chamber (**Figure 9**). Conversely a more reliable representation of the stone chamber extension along its main axis was obtained by the 3D inversion (**Figure 11a**) more correctly interpreting the profiles acquired parallel to the stone chamber. With this respect in **Figure 13** the results obtained from the 2D interpretation of the three survey lines (TK2, 3 and 5) parallel and near to the stone chamber are reported in a 3D representation obtained with Voxler. From this results it can be observed that the 2D profile just above the stone chamber (TK2) is limited in length, and consequently in depth of investigation, due to the available space on the top of the mound, and recognize therefore an increase in resistivity only in the upper portion of the stone chamber. The two other profiles in similar direction on the sides of the stone chamber (TK3 and TK5) are not exactly over the void and stone blocks of the chamber, nevertheless correctly report an increase in resistivity due to the stone chamber, and the presence of the natural hill below it. However the increase in resistivity observed from the 2D lines is lower with respect to the one inverted from the 3D model (**Figure 11a**) which, merging the information of the three lines and more correctly interpreting the 3D current flux distribution, allow for a more precise location and definition of the stone chamber in the longitudinal direction.
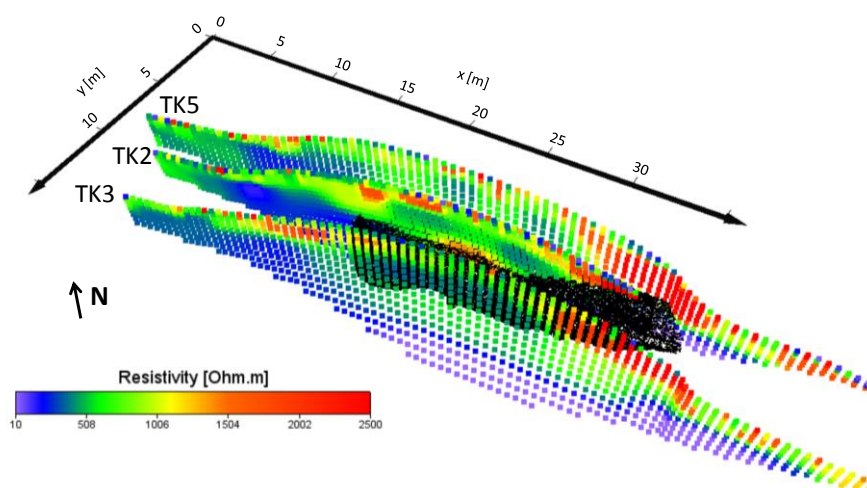

Figure 13: 3D visualization of the 2D interpretation of the three survey lines (TK2, 3 and 5) parallel and near to the stone chamber.

The 3D inversion was also highly valuable to depict a correct horizontal distribution of anomalies (**Figure 11b**). The 3D dataset was also obtained with a quite dense but not completely regular electrode disposition (see **Figure 4b**). This surveying approach was chosen for its ease of disposition on the ground and for its convenience in terms of time of the surveys. Particularly a full 3D acquisition (including cross cable measurements) was considered not feasible given the time available for the surveys and the dense vegetation over the mound. Comparative literature tests, performed by means of synthetic examples and field data (Tsourlos et al., 2014), verified the superiority of the radial disposition in delineating bodies positioned in the central part of a burial mound, as usually is the case for the stone chamber within Kofuns. The combined use of radial and transversal lines in the present survey seems to produce satisfactory results with a limited time increase for data acquisition and processing. Therefore a similar electrode disposition is in our opinion advisable for future investigations in similar environments. To better evaluate the potentiality of the chosen acquisition approach the 3D model sensitivity deriving from it is represented in **Figure 14** in normalized values with respect to the maximum sensitivity.
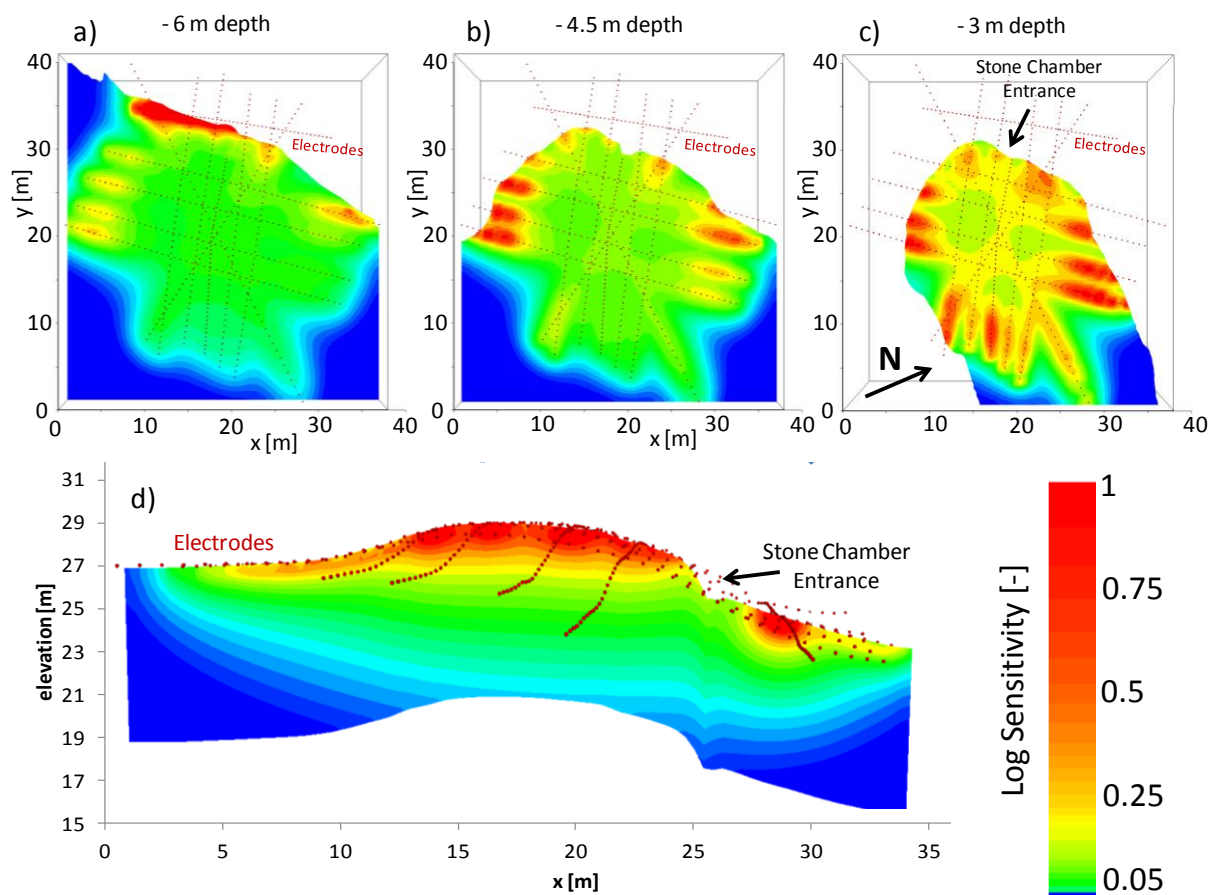

Figure 13: Sensitivity of the chosen electrode disposition: a), b) and c) map views at different depths from the top of the mound; d) section in correspondence of the middle of the stone chamber.

The sensitivity shows how much a resistivity change in a block of the model affects the potential readings. The higher the sensitivity, the more reliable is the final resistivity value of the block. The sensitivity can be computed as the square roots of the values of the diagonal of the $J^T * J$ matrix, where J is the Jacobian (i.e. the matrix of the derivatives of the data with respect to the resistivity of each model block; ^{T} indicates transpose). Sensitivities above a 0.01 threshold (1% of the maximum) are usually considered as significantly influencing the measurements.

From **Figure 14** it is possible to observe that the sensitivity of the model can be considered satisfactory till the desired investigation depth. Clearly the sensitivity is driven by profiles separation and orientation, being higher in correspondence of the survey lines and partially driving therefore the resolution of the model at the borders of the map (see **Figure 14b**). Nevertheless a satisfying coverage is obtained in the center of the model in correspondence of the location of the stone chamber (see **Figure 14c**). Also considering this sensitivity map however the choice of a smoothness constrain for 3D inversion was considered with respect to a robust constrain. This last would indeed produce undesired artefacts in the inversion given the partially reduced cross line sensitivity.

A part from the known stone chamber ERT surveys were also very important in defining the relationship between the chamber itself and the surrounding material. The abrupt lateral and vertical transition from the stone chamber to the sourrounding hill (**Figure 9**) may suggests that the stone chamber was excavated within the natural hill which could be composed of sandy-silty material, given the resistivity ranges evidenced. Moreover, the shallow coverage evidenced by the surveys (**Figure 9**) could be interpreted to be related to anthropic material, having a coarser nature with respect to the one of the natural hill, put in place to recover the excavated stone chamber. Alternatively this layer could be related to the reduced water content of the shallow part of the mound with respect to its lower part or to the presence of roots of the threes. If confirmed of anthropic origin the above mentioned evidence could give an insight on the construction procedure adopted for the Kofun.

Finally in **Figure 15** the main results of the surveys executed over the mound are reported with a representation based on high amplitude and high resistivity values of the investigated volume. From this figure it can be further evidenced the continuity of the high amplitude and high resistivity anomalies around the mound along an approximated circular pattern (dashed black line). These anomalies appear to be located in the changing slope position of the mound and therefore could suggest the presence of stone boulders put in place along the top ring of the mound to form a crown protecting ring and to preserve the mound shape. Similar construction peculiarities have been evidenced in some Kofuns such as the Teraguchi-Oshimi H-27 in Nara prefecture (Shinjo-cho Board

of Education and Archaeological Institute of Kashihara, Nara prefecture, 1988) and the Takennouchi No.3 in Hyogo prefecture (Youka-cho Board of Education, 2000).
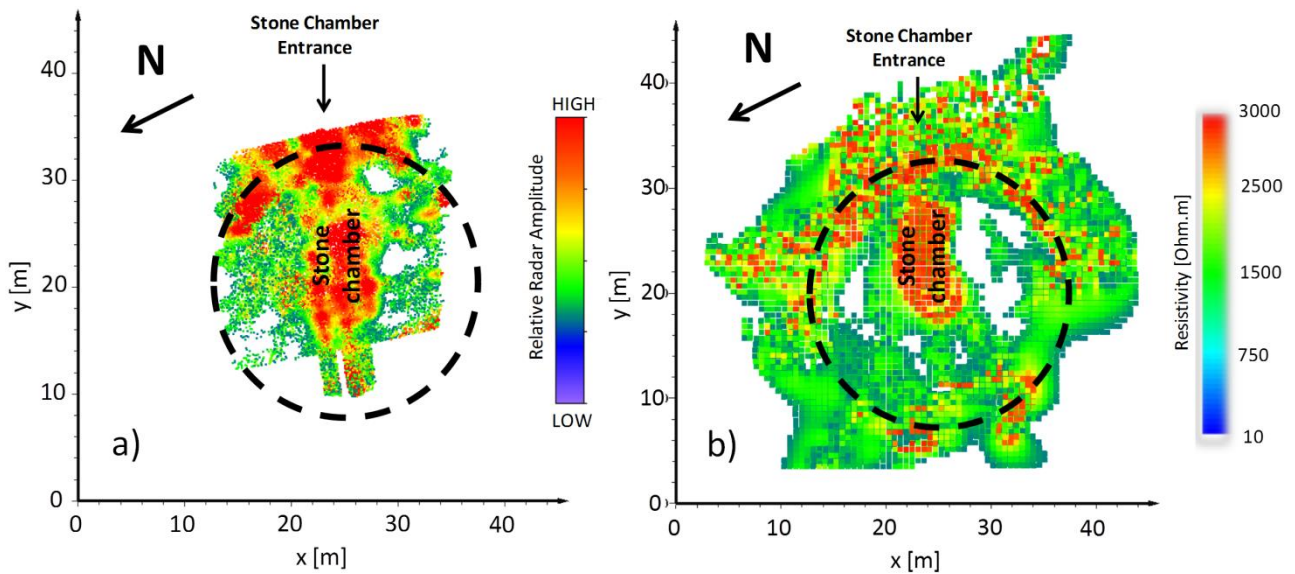

Figure 15: Main geophysical surveys results over the mound: a) GPR surveys with GPR amplitude map, cut to high amplitudes threshold; b) ERT surveys with 3D resistivity map, cut to high amplitudes threshold. In a) and b) the stone chamber location and the anomaly discussed in the text are evidenced.

7. CONCLUSIONS

Geophysical surveys reported in this paper were highly effective in delineating the investigated Tobiotsuka Kofun structure and in providing clear evidence of the relevant stone chamber peculiarities. Also, interesting geophysical anomalies were evidenced and potentially interpreted in term of archaeological significance. Geophysical results demonstrated the effectiveness of the chosen surveying approach in this particular environment. Similar survey disposition could be adopted in the investigation of comparable burial mounds in Japan or in other part of the world.

With respect to the major aims of the geophysical investigations it can be therefore stated that:

(i) the structure of the burial mound has been effectively reconstructed and hypothesis on the construction stages were performed;

(ii) the chosen ERT survey design with a combination of parallel and radial lines was provided effective in identifying the stone chamber structure and stone chamber wall thickness which was also confirmed by means of high resolution GPR surveys;

(iii) the surveys performed along the stone chamber floor suggested a clear preferential archaeological excavations location in the center end of the burial chamber.

Hypothesis on the nature of the anomalies evidenced by the geophysical surveys, which are reported in the paper, can be only speculative at this stage of research and need a direct verification by means of excavations. Ground truth will verify the effectiveness of geophysics in a rather difficult environment. Devoted excavations are planned in the next months and will be object of a future paper.

REFERENCES

1. Akagi Tsuyoshi (1927) - Geological Sheet Map 1:75,000, F. 220 – OKAYAMA, Geological Survey of Japan.

2. Barret, J.C., 1990.The monumentality of death: The character of early Bronze Age mortuary mounds in southern Britain. World Archaeology, 22(2), 179-189.

3. Bradley, R. and Fraser, E. (2010) Bronze age barrows on the heathlands of southern England: Construction, forms and interpretations. Oxford Journal of Archaeology, 29(1): 15–33.

4. Chen, R., Tian, G., Zhao, W., Wang, Y., Yang, Q. (2018) Electrical Resistivity Tomography with Angular Separation for Characterization of Burial Mounds in Southern China, Archaeometry, 60 (5), pp. 1122-1134.

5. Constable, S.C., Parker, R.L., Constable, C.G., 1987. Occam's Inversion: a practical algorithm for generating smooth models from EM sounding data. Geophysics, 52: 289–300.

6. Deckers, J.A., Driessen P., Nachtergaele, F., Spaargaren, O. (2001). World Reference Base for Soil Resources - in a nutshell, European Soil Bureau - research report no. 7.

7. Edwards, W., Okita, M., Goodman, D., 2000. Investigation of Subterranean Tomb in Miyazaki, Japan. Archaeological Prospection 7, 215–224.

8. Forte, E., and Pipan, M., (2008) Integrated seismic tomography and ground-penetrating radar (GPR) for the high-resolution study of burial mounds (tumuli), Journal of Archaeological Science, 35, 2614–2623.

9. Goodman, D., Nishimura, Y., 1993. A ground-radar view of Japanese burial mounds. Antiquity, 67, 349-354.

10. Goodman D., Nishimura Y. and Rogers J.D. (1995) GPR time slice in archaeological prospection. Archaeological Prospection, vol. 2, n. 2, pp. 85-89.

11. Goodman, D. (2004) GPR-SLICE. Ground Penetrating Radar Imaging Software. User's Manual, Geophysical Archaeometry Laboratory, California, 2004 (http://www.gpr-survey.com/practice/GPR-SLICE).

12. Goodman D., Steinberg J., Damiata B., Nishimura Y., Hongo H., Higashi N. and Schneider K. (2006) GPR Overlay Analysis for Archaeological Prospection, Proceedings of International Conference on Ground Penetrating Radar, Ohio State University.

13. Goodman D., Hiromichi H., Higashi N., Nishimura Y., Tokuda M. and Oh Hyun dok (2009) The application of GPR Overlay analysis in archaeological prospection: Discovery at the Japanese Imperial Family tombs in Miyazaki Prefecture, ArcheoSciences, Revue d'archéométrie 33 (suppl.) Mémoire du sol, espace des hommes.

14. Hodder I. (1984) Burials, houses, women and men in the European Neolithic D. Miller, C. Tilley (Eds.), Architecture and Order, Basil Blackwell, Oxford (1984).

15. Kamei, H., Marukawa, Y., Kudo, H., Nishimura, Y., Nakai, M., 2000. Geophysical survey of Hirui-Otsuka mounded tomb in Ogaki, Japan. Archaeological Prospection 7, 225–230.

16. Kipfer, B.A., 2000. Encyclopedic Dictionary of Archaeology. Kluwer Academic/Plemun.

17. Knoph T., Steinhaus W., Fukunaga S. ed.(2018) Burial Mounds in Europe and Japan: Comparative and Contextual Perspectives, Arcaeopress Publishing.

18. LaBrecque, D.J., Miletto, M., Daily, W., Ramirez, A., Owen, E., 1996. The effects of noise on Occam's Inversion of resistivity tomography data. Geophysics, 61: 538–548.

19. Matsuura Hirohisa, Chikao Kurimoto, Fumio Yoshida, Yoshiki Saito, Hiroshi Makimoto, Seiichi Toshimitsu, Toshimitsu Iwaya, Masao Komazawa and Toshio Hiroshima (2002) geological map of japan 1:200,000, ni-53-27, okayama and marugame, geological survey of japan.

20. Morelli, G., LaBrecque, D.J., 1996. Advances in ERT inverse modelling. European Journal of Environmental and Engineering Geophysical Society, 1 (2): 171–186.

21. Nishimura, Y., et al. 1993. Archaeological Prospecting. The Excavation Report of Nagatsuka Burial Mound Kofun, The Board of Education of Ogaki city, 20-54.

22. Nishimura, Y., Goodman, D., 1998. GPR as an imaging technique for subterranean features. International Archives of Photogrammetry and Remote Sensing, Vol. XXXII, Part 5, Hakodate.

23. Niiro, I. ed. (2012) Report of an investigation on the Zozan Kofun group, Okayama City. Report of Scientific Research (A), JSPS Grants-in-Aid for Scientific Research 2008-2011. Graduate School of Humanities and Social Sciences, Okayama University. [Japanese]

24. Papadopoulos N.G., Yi Myeong-Jong, Kim Jung-Ho, Tsourlos P., Tsokas G.N. (2010), Geophysical investigation of tumuli by means of surface 3D Electrical Resistivity Tomography, Journal of Applied Geophysics, 70, 192–205.

25. Pipan, M., Baradello, L., Forte, E., and Finetti, I., 2001, Ground penetrating radar study of Iron Age tombs in southeastern Kazakhstan, Archaeology Prospection, 8, 141–55.

26. Renfrew C., Bahn P. (2000) Archaeology: Theories, Methods, and Practice (third ed.), Thames & Hudson (2000).

27. Seike A., Yotsuda H. (2019) Tobiotsuka Kofun I : The survey of a burial mound with a huge stone chamber. The department of Archaeology, Okayama University[Japanese]

28. Shinjo-cho Board of Education and Archaeological Institute of Kashihara, Nara prefecture, (1988) Teraguchi-Oshimi Burial Mounds. Shinjo-cho Board of Education, Katsuragi. [in Japanese].

29. Steinhaus, W. and Knopf, T., 2018. Burial mounds in Europe and Japan: An introduction. In Knopf, T., Steinhaus, W. and Fukunaga, S.（Eds.), Burial Mounds in Europe and Japan: Comparative and Contextual Perspectives, Archaeopress Publishing Ltd: Oxford, pp. 1-15.

30. Suzuki Shigeyuky (1996) – Paleogene talus deposits, Okayama City, Southwest Japan. Okayama University Earth Science Reports, Vol 3, No. 1, 17-24.

31. Tembata H., (2016), Landscape analysis of tombs of the final kofun period in the kawachi area using a three-dimensional model, Archi-Cultural Interactions through the Silk Road, 4th International Conference, Mukogawa Women's Univ., Nishinomiya, Japan, July 16-18, Proceedings.

32. Tikhonov, A.N., Arsenin, V.Y., 1977. Solutions of ill-posed problems. Winston and Sons, Washington DC. 258 pp.

33. Tilley, C., 1994. A Phenomenology of Landscape: Places, Paths and Monuments. Berg.

34. Tonkov, N., Loke, M.H., 2006. A resistivity survey of a burial mound in the "Valley of the Thracian Kings". Archaeological Prospection 13, 129–136.

35. Tsourlos P., Papadopoulos N.G., Yi Myeong-Jong, Kim Jung-Ho, Tsourlos P., Tsokas G.N. (2014), Comparison of measuring strategies for the 3-D electrical resistivity imaging of tumuli, Journal of Applied Geophysics, 101, 77–85.

36. Tsude H. (1987) The Kofun Period. Recent Archaeological Discoveries in Japan. The Centre for East Asian Cultural Studies and UNESCO:pp.55-71.

37. Youka-cho Board of Education (2000) Takenouchi Burial Mounds, Youka-cho Board of Education, Youka. [in Japanese].

38. Zhao, W., Forte, E., Levi, S. T., Pipan, M., and Tian, G., 2015, Improved high-resolution GPR imaging and characterization of prehistoric archaeological features by means of attribute analysis, Journal of Archaeological Science, 54, 77–85.